Magneto-optical characterizations of inhomogeneities in $Bi_2Sr_2CaCu_2O_{8+y}$ single crystals grown by floating-zone method

M. Yasugaki,[1] M. Tokunaga,[1,2] N. Kameda,[1] and T. Tamegai[1,2]
[1]*Department of Applied Physics, The University of Tokyo, Hongo, Bunkyo-ku, Tokyo 113-8656, Japan*
[2]*CREST, Japan Science and Technology Corporation (JST), Japan*
(Received 19 November 2002; published 6 March 2003)

Magneto-optical observations of distribution of vortices and vortex-lattice melting transition fields are used to characterize the inhomogeneities in high-quality $Bi_2Sr_2CaCu_2O_{8+y}$ single crystals grown by the floating-zone method. Two kinds of characteristic features are found; one with expansion of vortex liquid phase forming arclike regions, and another with linear structures which are observed only in the vortex solid phase. The former is found to be related to the compositional inhomogeneities of the crystal, while the latter is related to the structural defects, most probably small angle grain boundaries. The origin of different evolutions of the vortex liquid region upon increase in the applied field is explained based on the sample-size dependent field profile in the crystal.

DOI: 10.1103/PhysRevB.67.104504 PACS number(s): 74.72.Hs, 74.25.Ha, 74.25.Dw

$Bi_2Sr_2CaCu_2O_{8+y}$ (BSCCO) is one of the most thoroughly studied high-temperature superconductors because of its extremely large anisotropy, easy cleavage nature, and highly stable surface conditions. Macroscopic measurements such as transport and magnetic studies rely on the homogeneity of the sample. However, not much works have been done on the characterization of the homogeneity of BSCCO crystals partly because of the lack of proper probes for its characterization. Inhomogeneities and defects in high-temperature superconductors influence the distribution of vortices and phase transitions of the vortex systems. Twin boundaries in $YBa_2Cu_3O_{7-y}$ (YBCO) are known to play an important role to determine vortex penetration into the crystal.[1] The existence of well-defined first-order vortex-lattice melting is also deeply affected by the presence of twin boundaries.[2] It is reported by magneto-optical (MO) observations in BSCCO that the vortex-lattice melting field shows large spatial variations.[3] On the other hand, inhomogeneities of microscopic scale are also reported by the state-of-the-art scanning tunneling microscopy by Pan *et al.*[4] They report that the superconducting gap in BSCCO has a large variation with characteristic length of about 20 Å. It is needless to say that correct physical pictures of the superconductivity can only be obtained by taking into account the real nature of the materials. In this paper we characterize high-quality BSCCO single crystals using differential MO technique in terms of the spatial distributions of vortices and the vortex-lattice melting field.

The crystals used in the present study are grown by the floating-zone method using an image furnace. They are subsequently annealed under controlled atmosphere to be optimally doped with $T_c = 91.7$ K and $\delta T_c < 1.5$ K.[5] These crystals are carefully cleaved to the thickness of about 30 μm and cut into approximate dimensions of $500 \times 400 \times 30$ μm^3 using a wire saw. We always cut the crystal so that the edges are either parallel or perpendicular to the growth direction of the crystal (a axis). In some cases, one of the corners is intentionally removed for easier identification of the orientation of the crystal. Differential MO images are taken by subtracting images at $H = H_a + \delta H_a/2$ from $H = H_a - \delta H_a/2$ with $\delta H_a \sim 1$ Oe.[3] To enhance signal-to-noise ratio, we average at least 100 differential images. Details of the method can be found in Refs. 3 and 6. Chemical compositions of the selected areas are analyzed for some of the crystals using wavelength dispersive x ray analyses after MO observations. We employ point analysis mode and accumulate x rays for 100 sec for each 10×10 μm^2 region. Since we are interested in the relative change of the cation composition, no absolute value calibrations are made.

Due to large thermal fluctuations, vortex lattice melts into vortex liquid upon increase of temperature and/or magnetic field.[7] Figures 1(a), 1(b), 1(d), 1(f), and 1(g) shows the differential MO images for BSCCO-*A* ($500 \times 390 \times 30$ μm^3) at 70 K near the bulk vortex-lattice melting transition field. Due to the presence of the vortex dome induced by geometrical barrier in a thin superconductor,[8] the vortex-lattice melting starts close to the center of the crystal [Fig. 1(a)].[3] The bright regions in Fig. 1 correspond to those experienced larger change in the local magnetic induction upon increase of the field by δH and hence are considered to be newly melted regions. The vortex-liquid region (vortex puddle), which is enclosed by the solid-liquid boundary, expands upon increasing the field as shown in Fig. 1(b). In an ideal case of a homogeneous thin superconductor, the vortex puddle is expected to expand keeping the nearly oval boundary. However, the boundaries in Figs. 1(b), 1(d), 1(f), and 1(g) display rather complex patterns. Such a nonideal expansion of liquid-solid boundary has been reported.[3,6,9,10] The thickness of the vortex liquid-solid boundary tells us how the vortex-lattice melting evolves locally. In the region where the boundary is fat, the boundary has moved a lot with the increment of field δH, while in regions where it shows discontinuity, the propagation of the interface is pinned. Though the crystal is high quality judging from the sharp transition width $\delta T_c \sim 1.5$ K, and the small rocking curve width $\delta\theta \sim 0.1°$, there must be inhomogeneities of some kind to account for the above behavior of the boundary. Local variation of the chemical composition and/or oxygen content is a possible

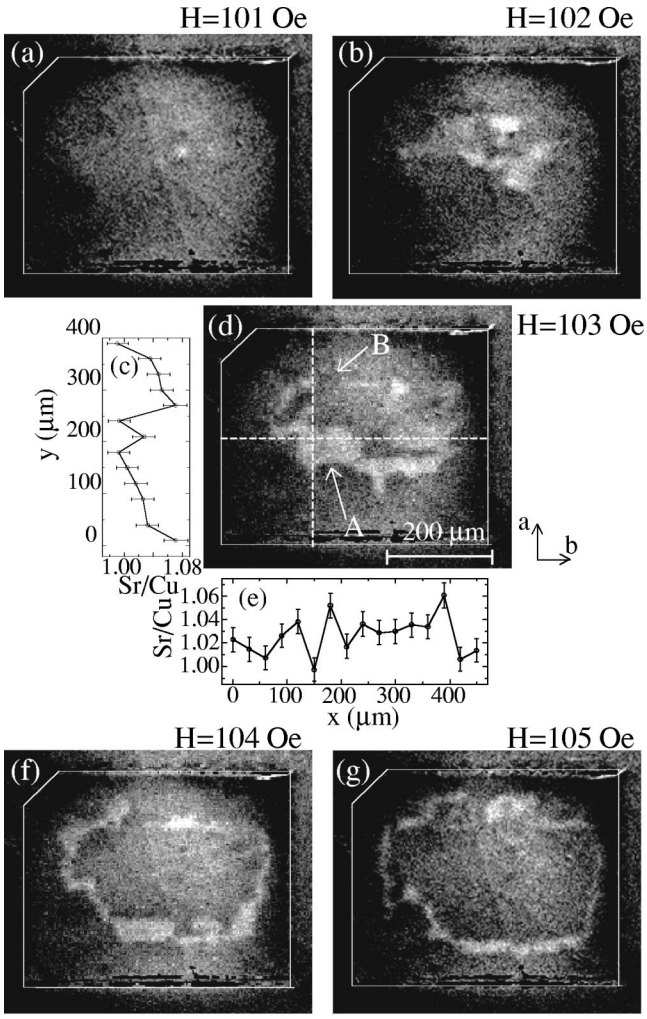

FIG. 1. Differential MO images for BSCCO-*A* at $T=70$ K near the vortex-lattice melting transition field (a) 101 Oe, (b) 102 Oe, (d) 103 Oe, (f) 104 Oe, and (g) 105 Oe. Positional dependence of strontium versus copper ratio on (c) vertical and (e) horizontal broken lines in (d). Vortex solid-liquid boundaries show large motion and pinning at points *A* and *B* in (c), respectively.

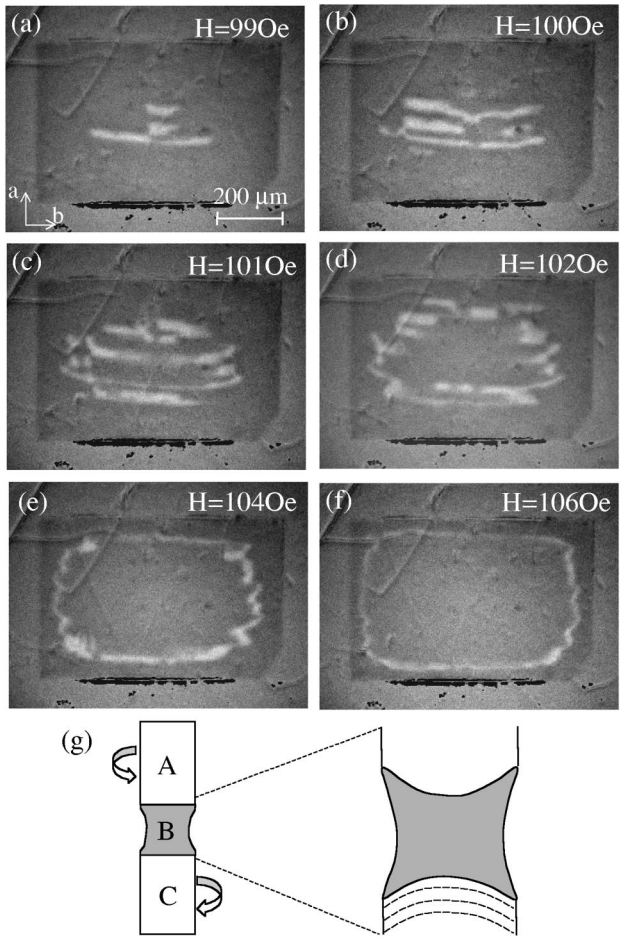

FIG. 2. Differential MO images for BSCCO-*B* at $T=70$ K near the vortex-lattice melting transition field (a) 99 Oe, (b) 100 Oe, (c) 101 Oe, (d) 102 Oe, (e) 104 Oe, and (f) 106 Oe. Vortex-lattice melting proceeds along lines nearly perpendicular to the *a* axis forming arclike structures. (g) Schematic drawing of the crystal growth process in the floating-zone method (left panel). Counter rotating feed rod (*A*) and grown crystal (*C*) sustain molten zone (*B*) by surface tension. The right panel shows schematic expanded cross-sectional view of the molten zone. The growth front is curved by the thermal gradient. Arclike structures (broken lines) seen by MO observations run parallel to the growth front.

candidate for such inhomogeneities. In order to map out possible variation of chemical compositions, detailed chemical analyses on selected regions of the crystal are performed. Figures 1(c) and 1(e) show the spatial variations of the ratio of strontium to copper (Sr/Cu) along horizontal and vertical broken lines in 1(d), respectively. The Sr/Cu ratio shows noticeable variation in this small crystal. The location of the large variation of the Sr/Cu ratio seems to closely match the region where vortex solid-liquid interfaces show large motion (point A) or sign of pinning (point B). The ratios of other cation elements show similar variations with reduced magnitude. It is difficult, however, to determine how the local doping level changes with the change in Sr/Cu ratio, since it is determined by the charge balance of all the elements including oxygen, which is not analyzed here.

Figures 2(a)–2(f) shows other typical examples of the evolution of vortex solid-liquid boundaries in BSCCO-*B* ($700\times500\times30\ \mu m^3$). Here, the vortex liquid region expands forming a lot of linear structures nearly parallel to a specific direction of the crystal, which is confirmed to be perpendicular to the *a* axis. Close inspection of these linear features shows that they are not completely straight but are arclike with their radius of about 10 mm. A hint for such a shape comes from the fact that the crystal grows along the *a* axis. Namely, the arclike structures run nearly perpendicular to the growth direction. During the crystal growth by the floating-zone method, molten zone separates the polycrystalline feed rod and the grown single crystal of about 6 mm in diameter as shown schematically in the left panel of Fig. 2(g). The curvature of arclike structures is nearly equal to that of boundary between molten zone and the grown crystal

[right panel of Fig. 2(g)]. In the case of crystal growth from liquid phase such as floating-zone method and Czochralski method, the presence of striation is well-known. In impurity-doped Si (Ref. 11) and GaAs,[12] the striation consists of periodic modulation of dopant concentrations. The striation can occur due to the rotation of the crystal during the growth. In this case the spacing of the striation agrees with the growth length of the crystal per rotation of the crystal. On the other hand, it can also arise from temperature fluctuations due either to thermal convection or to Marangoni convection. Temperature fluctuations can lead to the change in the equilibrium composition in the melt. Since the crystallization front between the crystal and the melt is curved as shown in the schematic cross-sectional view in the right panel of Fig. 2(g), the equi-chemical composition line would be also curved. Since the time scale for the instability is of the order of seconds, the striation has characteristic length scale of about 10 μm at a typical growth speed of 20 mm/h for semiconductors. However, in our growth condition of BSCCO crystals, the growth rate is 0.2 mm/h which is two orders of magnitude slower than the typical growth rate in the floating-zone method. Hence, we expect that the characteristic length for the compositional variation based on this mechanism is much shorter. In the steady state of the crystal growth, the composition of the molten zone should stay constant. However, extremely slow crystal-growth rate inevitably induces temperature fluctuations of the molten zone since we only control the halogen lamp power in the floating-zone method. Variation of circumstances around by the floating-zone furnace such as changes in the ambient temperature could result in the temperature fluctuations of the molten zone. For example, our BSCCO crystal grows about 17 μm in 5 min, which is a typical time scale for the fluctuation in ambient temperature. This value is comparable to the spacing of the arclike structures in the vortex liquid region. It should be noted that the motion of the translation mechanism of the mirrors in the floating-zone furnace is found to have negligible irregularity and can be excluded as a possible origin of the arclike structures.

Figure 3 shows another typical example of the pattern observed in the differential MO images in BSCCO-*C* ($500\times800\times30$ μm^3). Straight lines parallel to each other can be identified in the vortex solid phase below $H\leqslant42$ Oe as in Figs. 3(a)–3(c). The direction of these straight lines are always nearly parallel to the *a* axis, which is the growth direction of BSCCO crystals. Such straight defects could be related to the crystal defects, most probably, the small angle grain boundaries. It is very difficult to make the grown BSCCO crystal into one single crystal, unlike the case of $La_{2-x}Sr_xCuO_4$.[13] BSCCO crystals usually grow along the *a* axis with medium size crystallites whose *c* axes are rotated one to the others. This growth habit naturally produces a lot of small-angle [001] tilt grain boundaries. In MO observations, we select a flat part of the crystal with no visible defects on both surfaces and cut it into rectangular shape. However, we cannot completely exclude the possibility to have small angle grain boundaries with very small misorientation buried in the crystal. Small angle grain boundaries in BSCCO are reported to be a channel for vortex motion[14]

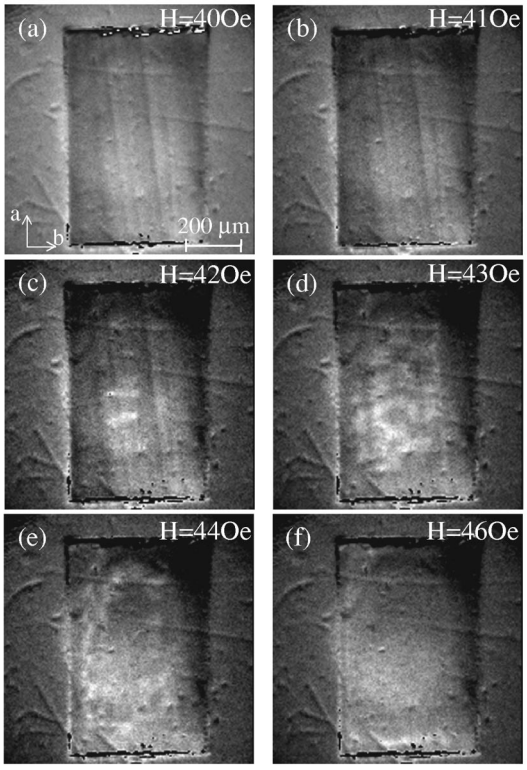

FIG. 3. Differential MO images for BSCCO-*C* at $T=70$ K below the vortex-lattice melting transition field (a) 40 Oe, (b) 41 Oe, (c) 42 Oe, (d) 43 Oe, (e) 44 Oe, and (f) 46 Oe. Several straight lines having different contrast from the rest of the region can be identified in the vortex solid state (a)–(c).

such as twin boundaries in YBCO.[1] Straight lines in the vortex solid phase are observed only in a small number of crystals. This is in contrast to arclike structures or irregular solid-liquid boundaries, either one of which is always observed.

Vortex solid-liquid boundaries in BSCCO grown by the floating-zone technique always show irregularities of some kind. The pattern depends on the size of the crystal. Namely, when the sample is large, the solid-liquid boundary shows arclike structure, while it shows oval shape with some irregularities when the sample is small. When the magnetic field is applied along the *c* axis in thin BSCCO crystals, vortex penetration is delayed by the geometrical barrier which is supported by the shielding current at sample edges. The flux profile of such a sample is determined by the width-to-thickness ratio w/t of the sample. Figure 4(a) shows the calculated field profile for thin infinite strips with various widths and a fixed thickness of 30 μm. We assume the edge shielding current flows only in the regions within half the thickness from the edges. In a sample with small width, the edge current occupies a large portion of the sample and flux profile becomes steep as shown by inverted solid triangles in Fig. 4(a). By contrast, the flux profile in a sample with large width has a large flat region near the center of the sample [solid circles in Fig. 4(a)]. BSCCO crystals have a spatial modulation of the cation composition as we have shown already, which leads to the modulation of the melting field. As

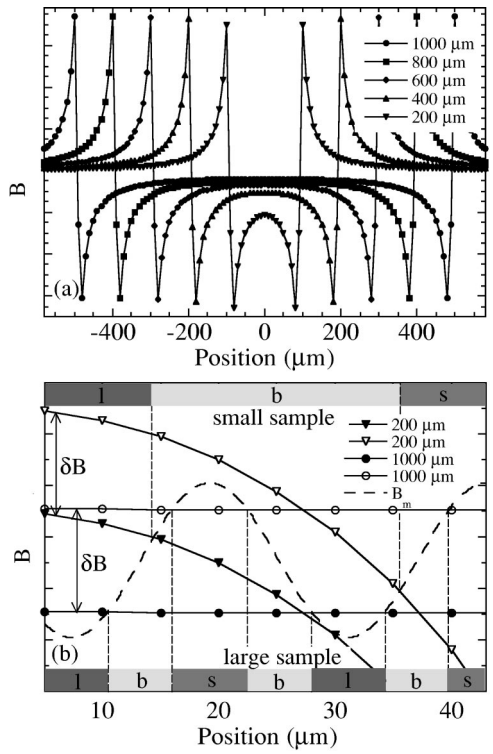

FIG. 4. (a) Calculated field profile for thin infinite strip superconductors with different widths in the presence of geometrical barrier. The thickness of the sample is fixed to 30 μm. (b) Examples of the evolutions of melting pattern upon increasing the local induction by δB for the small (inverted triangles) and large samples (circles). Due to the intrinsic spatial variation of the melting field, the size and the number of the liquid (l), boundary (b), solid (s) regions change.

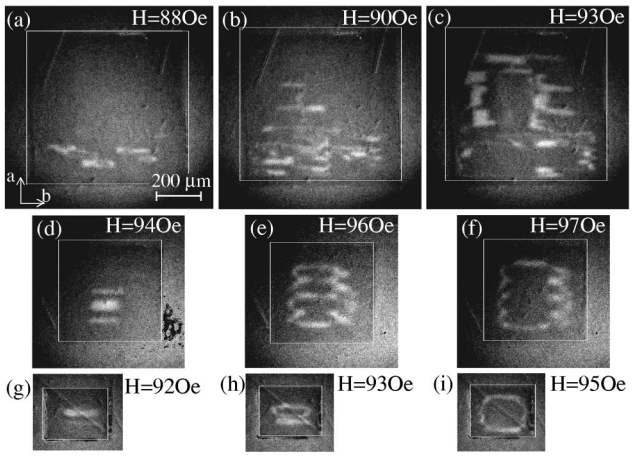

FIG. 5. Differential MO images at $T=70$ K near the vortex-lattice melting transition field $H=92$ Oe for crystals with different dimensions (D1,D2,D3). As the size of the crystal becomes smaller, the vortex solid-liquid boundaries change their shapes from irregular linear pattern to oval shape.

an example, we superimpose the local variation of the melting field shown in the wavy broken line. The increase in field H by δH leads to multiple liquid (l), boundary (b), and solid (s) regions for a sample with small width, while there is one large liquid region for a sample with large width. This scenario is confirmed by systematic measurements of the sample size dependence of the melting patterns. We prepared three crystals by cutting one large single crystal BSCCO-D. Figures 5(a)–5(i) shows the vortex solid-liquid boundaries for these crystals (D1: $750\times690\times30$ μm^3, D2: $450\times450\times30$ μm^3, D3: $360\times290\times30$ μm^3). The change in the melting pattern with changes in the sample size is consistent with the above calculation. Namely, when the size of the sample is large as in Figs. 5(a)–5(c), vortex liquid regions nucleate at various locations in the sample and expand forming arclike structures. As the size of the sample is reduced, the number of nucleation points decreases and the arclike structures are connected to form a single or a small number of liquid puddles as shown in Figs. 5(d)–5(f). Further reduction of the size results in the nearly ideal shape of the vortex puddle [Fig. 5(i)].

How much the inhomogeneities presented in this paper affects macroscopic properties of BSCCO crystals, such as transport, thermal, magnetic properties are subject of future studies. For example, conflicting results on the in-plane anisotropy in BSCCO single crystals may, in part, find explanation based on the presence of inhomogeneities.[16–18] Another important issue is how much are these inhomogeneities intrinsic to BSCCO crystals grown by the floating-zone technique. Since there have been no reports of vortex-lattice melting transition in BSCCO crystals grown by methods other than the floating-zone or the traveling-solvent floating-zone techniques, we cannot comment whether it is intrinsic to the crystal growth technique or not. However, it is worth mentioning that Kasai *et al.* found one-dimensional arrangements of vortices in $(La_{1-x}Sr_x)_2CuO_4$ grown by the traveling-solvent floating-zone technique.[15] They observed vortex alignments along a specific direction of the crystal with typical spacing of about 50 μm using scanning SQUID microscopy.

Finally, the striation in semiconductors can be controlled to some extent by optimizing the growth conditions to minimize turbulent flow in the molten zone during the crystal growth. Similar optimization against temperature fluctuations and instabilities in the melt may work also in oxide material BSCCO. Studies along this line would be vital for the exploration of physical properties of high temperature superconductors not only for vortex physics but also for other more fundamental properties related to the mechanism of superconductivity.

In summary, intrinsic inhomogeneities and defects in high quality $Bi_2Sr_2CaCu_2O_{8+y}$ single crystals grown by the floating-zone technique are characterized by differential magneto-optical observations. An ideal vortex-lattice melting starting from the center of the sample with oval solid-liquid boundary is distorted by compositional modulations, which are most probably induced by the temperature fluctuations during the crystal growth. Another typical pattern of straight lines in the vortex solid state is discussed in relation with the

small angle grain boundaries which are invisible from the crystal surface. The evolution of the vortex-melting pattern with the size of the crystal is explained by considering the vortex dome profile in the crystal.

We thank F. Sakai and K. Itaka for technical assistance. This work was supported by a Grant-in-aid for Scientific Research from the Ministry of Education, Culture, Sports, Science and Technology.

[1] U. Welp, T. Gardiner, D. Gunter, J. Fendrich, G.W. Crabtree, V.K. Vlasko-Vlasov, and V.I. Nikitenko, Physica C **235-240**, 241 (1994).

[2] W.K. Kwok, S. Fleshler, U. Welp, V.M. Vinokur, J. Downey, G.W. Crabtree, and M.M. Miller, Phys. Rev. Lett. **69**, 3370 (1992).

[3] A. Soibel, E. Zeldov, M. Rappaport, Y. Myasoedov, T. Tamegai, S. Ooi, M. Konczykowski, and V.B. Geshkenbein, Nature (London) **406**, 282 (2000).

[4] S.H. Pan, J.P. O'Neal, R.L. Badzey, C. Chamon, H. Ding, J.R. Engelbrecht, Z. Wang, H. Eisaki, S. Uchida, A.K. Guptak, K.-W. Ngk, E.W. Hudson, K.M. Lang, and J.C. Davis, Nature (London) **413**, 282 (2000).

[5] S. Ooi, T. Shibauchi, and T. Tamegai, Physica C **302**, 339 (1998).

[6] M. Yasugaki, K. Itaka, M. Tokunaga, N. Kameda, and T. Tamegai, Phys. Rev. B **65**, 212502 (2002).

[7] E. Zeldov, D. Majer, M. Konczykowski, V.B. Geshkenbein, V.M. Vinokur, and H. Shtrikman, Nature (London) **375**, 373 (1995).

[8] E. Zeldov, A.I. Larkin, V.B. Geshkenbein, M. Konczykowski, D. Majer, B. Khaykovich, V.M. Vinokur, and H. Shtrikman, Phys. Rev. Lett. **73**, 1428 (1994).

[9] A. Soibel, Y. Myasoedov, M.L. Rappaport, T. Tamegai, S.S. Banerjee, and E. Zeldov, Phys. Rev. Lett. **87**, 167001 (2001).

[10] T. Tamegai, M. Yasugaki, K. Itaka, and M. Tokunaga, Physica C **357-360**, 568 (2001).

[11] A. Eyer and H. Leiste, J. Cryst. Growth **71**, 249 (1985).

[12] H. Kohda, K. Yamada, H. Nakanishi, T. Kobayashi, J. Osaka, and K. Hoshikawa, J. Cryst. Growth **71**, 813 (1985).

[13] I. Tanaka and H. Kojima, Nature (London) **337**, 21 (1989).

[14] T. Egi, J.G. Wen, H. Kubota, J. Ricketts, and N. Koshizuka, Appl. Phys. Lett. **66**, 3680 (1995).

[15] J. Kasai, N. Okazaki, Y. Togawa, T. Sasagawa, J. Shimoyama, K. Kishio, H. Koinuma, and T. Hasegawa, Appl. Phys. A: Mater. Sci. Process. **72**, S263 (2001).

[16] S. Martin, A.T. Fiory, R.M. Fleming, L.F. Schneemeyer, and J.V. Waszczak, Phys. Rev. Lett. **60**, 2194 (1988).

[17] T. Motohashi, Y. Nakayama, T. Fujita, K. Kitazawa, J. Shimoyama, and K. Kishio, Phys. Rev. B **59**, 14 080 (1998).

[18] Y. Ando, J. Takeya, Y. Abe, X.F. Sun, and A.N. Lavrov, Phys. Rev. Lett. **88**, 147004 (2002).